FRACTURE TOUGHNESS DETERMINATION FOR A BERYLLIUM-BEARING BULK METALLIC GLASS

R.D. Conner, A.J. Rosakis*, W.L. Johnson, and D.M. Owen*
W.M. Keck Laboratory of Engineering Materials, 138-78
*Graduate Aeronautical Laboratories, 105-50
California Institute of Technology, Pasadena, California 91125

Introduction

A class of beryllium-bearing bulk metallic glass alloys has recently been developed at the California Institute of Technology (1). These alloys can be fabricated in the form of large ingots with minimum dimensions on the order of centimeters, which allows valid mechanical tests to be performed on these materials. Such tests were not formerly possible given the small dimensions of earlier metallic glass specimens. Some basic physical and mechanical properties have been measured on a specific beryllium-bearing bulk metallic glass with a nominal composition of $Zr_{41.25}Ti_{13.75}Cu_{12.5}Ni_{10}Be_{22.5}$ (2), by the authors and some of their co-workers. The results, which show the remarkable properties of such amorphous metals, are listed in Table 1. The purpose of this paper is to report on the first ever direct measurement of the fracture toughness of any bulk metallic glass system.

Experimental

Metallic glass ingots of the beryllium-bearing metallic glass with the composition of $Zr_{41.25}Ti_{13.75}Cu_{12.5}Ni_{10}Be_{22.5}$, were fabricated in the form of plates with approximate dimensions of $10 \times 100 \times 100$ mm. The impurities in the as-received raw materials, such as oxides, often act as nucleation sites for crystalline particles within the bulk metallic glass. The oxygen content of ingots fabricated for the present study is estimated as 800 ppm. A limited distribution of these crystalline particles with dimensions on the order of 10-20 μm were observed during preliminary investigation of the ingots using optical microscopy.

The Mode-I fracture toughness was measured by simultaneous use of two independent techniques. The optical method of CGS (3) and boundary value measurement. The fracture specimens were cut and ground to the dimensions shown in Table 2. The sample used in conjunction with CGS measurement was ground optically flat and polished to a highly reflective finish. Two independent techniques were used in order to increase the confidence in the fracture toughness measurement and to establish the

TABLE 1

Mechanical Properties of $Zr_{41.25}Ti_{13.75}Cu_{12.5}Ni_{10}Be_{22.5}$ Bulk Metallic Glass

Property	Value
Young's Modulus	96 GPa
Shear Modulus	34.3 GPa
Poisson's ratio	0.36
Tensile yield strength	1.9 GPa
Tensile strain to failure	2 %
Hardness (Vickers)	534 kg/mm^2
Thermal Expansion Coefficient	10.1x10^{-6}/°C
Density	6.11 g/cm^3

validity of CGS in performing this task. The use of optical techniques such as CGS becomes important in experimental situations where boundary value measurements are inadequate for inferring toughness (e.g. dynamic fracture).

Boundary Value Measurements

Mode I fracture toughness, K_{IC}, was determined using boundary measurements taken from specimen loading in 3-point bending configuration. Specimens were loaded until failure, and the corresponding K_{IC} value was calculated from (4)

$$K_I = \frac{P}{B\sqrt{W}} \frac{3\frac{S}{W}\sqrt{\frac{a}{W}}}{2\left(1+2\frac{a}{W}\right)\left(1-\frac{a}{W}\right)^{\frac{3}{2}}}\left[1.99-\frac{a}{W}\left(1-\frac{a}{W}\right)\left\{2.15-3.93\left(\frac{a}{W}\right)+2.7\left(\frac{a}{W}\right)^2\right\}\right] \quad (1)$$

The applied load is P, and dimensions a, W, B and S are defined in Table 2.

Figure 1 illustrates the typical variation of K_I with load point displacement δ, which has a peak value, K_{IC} = 59.5 MPa$\sqrt{m}$. It is interesting to note that the loading curve remains linear up until failure, suggesting very limited inelasticity. At failure, the crack propagation is unstable, indicated by the instantaneous unloading of the specimen. Results obtained from experiments conducted on 3 specimens gave consistent K_{IC} values of 55, 57 and 59.5 MPa$\sqrt{m}$. For valid plane strain fracture toughness testing, the specimen thickness must be greater than $2.5(K_{IC}/\sigma_o)^2$ where σ_o is the yield stress. Typical values for the metallic glass of $K_{IC} \sim 57$ MPa$\sqrt{m}$ and $\sigma_o \sim 2$ GPa, requires that the specimen thickness be greater than ~1.6 mm for plane strain conditions. Specimens used in the present study were at least 2.2 mm thick and therefore the results reported represent the plane strain fracture toughness of the metallic glass.

TABLE 2

Fracture Sample Dimensions

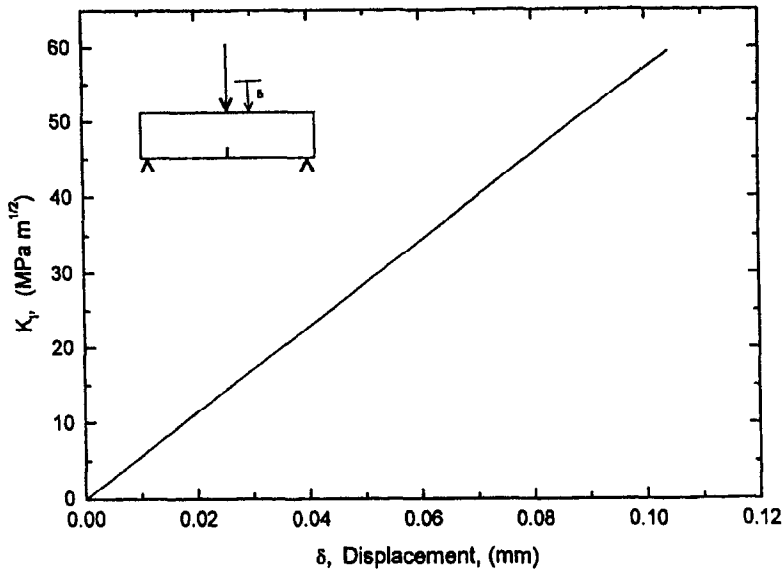| Dimension (mm)	Boundary-value samples	CGS sample
Length, L	50.8	112
Width, W	12.6	40.8
Thickness, B	2.2	4.8
Notch length, a	3	11.6
Loading span, S	46	104.2

Figure 1. The variation of K_I with load point displacement for a specimen loaded quasistatically in a three point bend configuration.

Coherent Gradient Sensing (CGS)

CGS is a full field, lateral shearing interferometric technique with an on-line spatial filter. In the reflection mode the technique measures out-of-plane displacement gradients (surface slopes). When the sample is loaded the surface deforms in the region near the crack tip, causing nonuniform spatial gradients in the optical path when light is reflected from its surface. The changes in the optical path are related to gradients in the stress state which are induced when loads are applied to the boundary of the initially undeformed specimen.
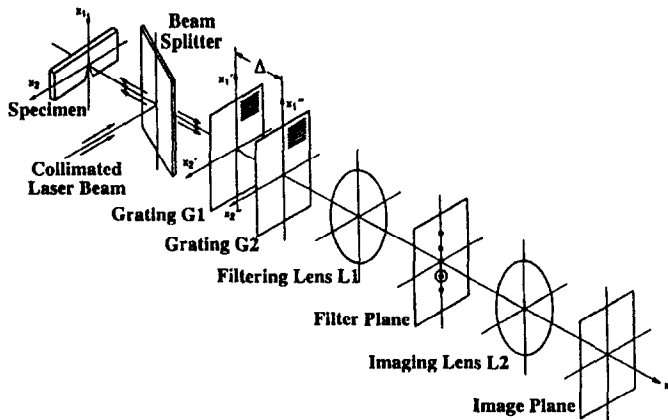

Figure 2. Schematic illustration of the experimental configuration for coherent gradient sensing (CGS) in reflection.

A schematic illustration of the experimental setup used for reflective CGS is shown in Figure 2. An optically flat, highly reflective plate specimen is illuminated by collimated coherent laser light. The reflected beam is then incident on a pair of gratings (40 lines/mm), G_1 and G_2, separated by a distance Δ. The field distribution on the G_2 plane is spatially filtered by the filtering lens L_1 and its frequency content is displayed on its back focal plane. By locating a filtering aperture around either ± 1 diffraction orders, information regarding the stress gradients is obtained on the image plane of the lens L_2. Complete details of the technique are given elsewhere (3).

Figure 3 is a photograph of CGS interference fringes on the metallic glass sample immediately prior to failure. The individual fringes in Fig. 3 represent contours of constant $\partial u_3/\partial x_1$. By measuring the values of the local polar coordinates r and ϕ for a specific fringe order, the out of plane deformations, and hence K_I, may be calculated from:

$$\frac{\partial u_3}{\partial x_1} = \frac{v\,h}{2E}\frac{K_1}{\sqrt{2\pi}}\,r^{-\frac{3}{2}}\cos\left(\frac{3}{2}\phi\right) = \frac{mp}{2\Delta} \qquad (2)$$

where u_3 is the deformation normal to the plane of the specimen, x_1 is the in-plane direction aligned with the crack, v is Poisson's ratio, h is the plate thickness, E is Young's modulus, m represents the fringe order, p is the diffraction grating pitch and Δ is the grating spacing. Measurements taken from Fig. 3, which was recorded just prior to crack initiation, provided a fracture toughness of $K_{Ic} = 55$ MPa√m. Figure 4 is a plot of K_I calculated from boundary measurements versus K_I measured from CGS. Note that these values are in agreement within 10%.

Given the extremely high yield stress and failure strength of The metallic glass, one might have expected the fracture toughness to be comparable to that of brittle ceramic materials. Such brittle solids have fracture toughness' typically less than 10 MPa√m and, as shown in Table 3, compare very unfavorably to structural metals (e.g. steels, aluminum, titanium) whose toughness' exceed 30 MPa√m. The metallic glass, however, exhibits toughness comparable to many high strength steels and approaches that of some titanium alloys.
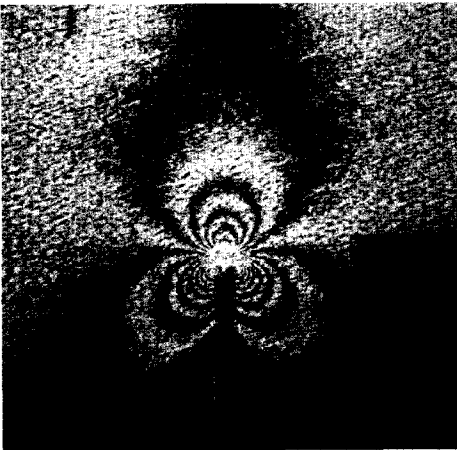

Figure 3. CGS pattern recorded from a metallic glass specimen loaded in three point bend.
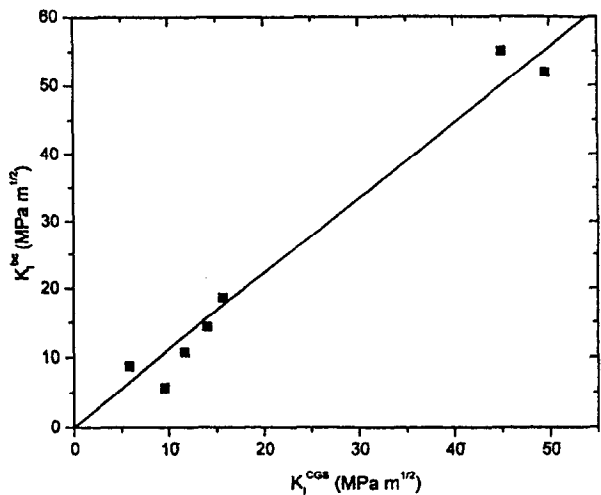

Figure 4. Comparison of the stress intensity factor determined from boundary value measurements with that determined using CGS.

TABLE 3
Fracture Toughness of Selected Engineering Materials (5)

Material	K_{IC} (MPa$\sqrt{m}$)
$Zr_{41.25}Ti_{13.75}Cu_{12.5}Ni_{10}Be_{22.5}$	55-59
Ti 6Al-4V	70-120
Polycarbonate	2.75-3.3
C300 maraging steel	50-70
2024 aluminum, T351	31-44
Al_2O_3	3-5.5
SiN_4	4.2-5.2
Electrical porcelain ceramics	1.03-1.25

The high fracture toughness points toward some microscopic toughening mechanisms. In ideally brittle fracture, the critical energy release rate under plane strain conditions, $G_{IC} = (1-v^2)K_{IC}^2/E$ simply equals the energy to create two free surfaces, $2\gamma_s$. Assuming brittle fracture, the apparent surface energy of the metallic glass can be estimated. Using $K_{IC} \sim 57$ MPa$\sqrt{m}$, E = 96 GPa and $v = 0.36$, the calculated apparent surface energy is almost 30,000 J m^{-2}. This apparent surface energy for the metallic glass is exceedingly high in comparison to measured surface energies of ceramics and pure metals which are typically 0.5-10 Jm^{-2}. This high apparent value of the surface energy may suggest the operation of other mechanisms in addition to surface creation that would contribute to a high net energy release rate.

Optical and scanning electron microscopy were used to investigate the microstructural processes associated with fracture in the metallic glass. Figure 5 shows a scanning electron micrograph of the fracture surface of a metallic glass specimen. The relatively smooth area on the left of the micrograph is the surface of the initial notch, whereas as the rougher region on the right side of micrograph is the fracture surface. In Fig. 5 there is no evidence of macroscopic shear lips adjacent to the plate specimen surfaces. The local roughness on the fracture surface is on the order of 50-150 μm. Figure 6 shows a optical micrograph of the crack profile of the mating half of the specimen shown in Fig. 5. The initial notch is located on the left of the micrograph. The small bright regions in the micrograph are crystalline particles which are embedded in the bulk metallic glass. Most crystallites in the region near the initial notch and adjacent to the crack path contain microcracks in the direction parallel to macroscopic
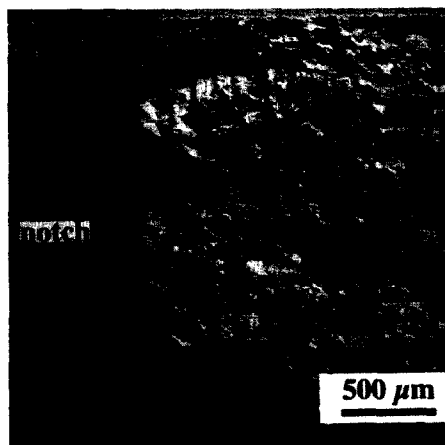

Figure 5. Scanning electron micrograph of the fracture surface of a metallic glass specimen. The initial notch is located to the left of the image.

Figure 6. Optical micrograph of the crack profile from the mating half of metallic glass specimen shown in Fig. 5. Regions of both slant fracture and flat fracture are observed. The initial notch is on the left of the micrograph.

crack growth (perpendicular to the direction of tensile loads induced by the crack). In some cases, crystallites located in the vicinity of the crack path were also surrounded by apparent microvoids. As illustrated in Fig. 6, the crack path exhibits essentially flat regions parallel to the macroscopic crack path and surfaces angled at 45° with respect to the crack path. Inspection of these regions along the entire length of the fracture surface indicated that the flat regions were often associated with the presence of fractured crystallites, whereas the ligaments in the region between the crystallites angled at 45° are reminiscent of void sheet formation in ductile metals. The maximum extent of the plane strain plastic zone size r_p, was estimated using the following relation

$$r_p\left(\frac{\pi}{2}\right) = \frac{1}{4\pi}\left(\frac{K_{IC}}{\sigma_o}\right)^2\left[(1-2v)^2+\frac{3}{2}\right] \approx 0.126\left(\frac{K_{IC}}{\sigma_o}\right)^2 \tag{3}$$

which resulted in a value of r_p = 102 μm. The calculated plastic zone size is approximately equivalent in size to the fracture surface roughness shown in Fig. 5.

Ongoing work by the authors in this area concentrates on the investigation of the effect of loading rate and metallic glass composition on fracture toughness.

References

1. A. Peker and W.L. Johnson, Applied Physics Letters 63, 2342 (1993).
2. H.A. Bruck, T. Christman, A.J. Rosakis, W.L. Johnson, *Scripta Metallurgica et Materialia* 30, 429 (1994).
3. A.J. Rosakis, in Experimental Techniques in Fracture (J.S. Epstein, ed.), p. 327, VCH Publishers, New York (1993).
4. T.L. Anderson, Fracture Mechanics, Fundamentals and Application. CRC Press, Boca Raton (1991).
5. R.W. Hertzberg, Deformation and Fracture Mechanics of Engineering Materials, John Wiley & Sons, New York (1988).